Proceedings of the ASME 2024 19th International Manufacturing Science and Engineering Conference
MSEC2024
June 17-21, 2024, Knoxville, Tennessee

MSEC2024-125256

BRIEF PAPER: PROCESS MONITORING AND FAULT DETECTION IN LASER POWDER BED FUSION USING IN-SITU ACOUSTIC EMISSIONS

Benjamin D. Bevans
Virginia Tech
Blacksburg, VA

Alexander Riensche
Virginia Tech
Blacksburg, VA

Yuri Plotnikov
CCAM
Disputanta, VA

John Sions
CCAM
Disputanta, VA

Kyle Snyder
CCAM
Disputanta, VA

Derek Hass
Commonwealth Center for Advanced Manufacturing (CCAM)
Disputanta, VA

Prahalada Rao
Virginia Tech
Blacksburg, VA

ABSTRACT

This work concerns process monitoring in the laser powder bed fusion additive manufacturing process. In this work, we developed and applied a novel in-situ solution for process stability monitoring and flaw detection using acoustic emission sensing. Current process monitoring methods in laser powder bed fusion only focus on the top surface of the deposition process, using an array of sensors to capture data on a layer-by-layer basis. Common sensors used for in-situ monitoring of the laser powder bed fusion process are optical, infrared, and high-speed imaging cameras along with pyrometers and photodiodes. A critical flaw with traditional top surface monitoring methodologies is that they are unable to reliably monitor the subsurface phenomena that occur in the laser powder bed fusion process. These subsurface effects are caused by the meltpool penetrating multiple layers below the top surface, leading to the re-solidification of the microstructure and potentially generating key-hole porosity. By only monitoring the top surface of the laser powder bed fusion process, the meltpool depth aspects and effects are ignored. To overcome the limitations of current in-situ monitoring of subsurface effects, this work utilizes four passive acoustic emission sensors attached to the build plate. These acoustic emission sensors monitor the energy emissions generated from the surface-level laser material interactions. Moreover, the acoustic emission signals are capable of traveling through the previously deposited layers, through the build plate, and to the sensors. Therefore, the acoustic waveform generated by the laser can capture process phenomena ranging from the crystallographic level to the macro-scale layer level which are at the root of flaw formation inside the deposited part. Hence, acoustic emission monitoring has the ability to monitor the subsurface effects in the laser powder bed fusion process. To monitor and analyze this acoustic waveform, novel wavelet-based decomposition is combined with heterogeneous sensor fusion to not only capture the acoustic waveform in time, but also in locational space on the build plate. Locational acoustic emission data enables the ability to determine the source of the generated acoustic waveform which is advantageous when the location of flaws is desired. This extracted spatially placed acoustic waveform data is able to detect the effect of processing parameters with a statistical fidelity of 99%. The proposed locational acoustic waveform monitoring method correlates to the resulting surface roughness of manufactured samples with a fidelity of 86%. Additionally, we show that acoustic waveform monitoring detects the onset of part failure, recoater crashes, and warpage prior a priori to the actual failure point.

Keywords: Additive manufacturing, acoustic emission, sensor data fusion, in-situ monitoring

1. INTRODUCTION

In the laser powder bed fusion (LPBF) additive manufacturing (AM) process, metal powder is raked across a build plate and selectively smelted using a laser [1]. The LPBF process is emerging as a favored method for manufacturing high-value, geometrically complex, and high-performance parts [2]. This process is particularly favored in industries such as automotive, aerospace, energy, and biomedical due to its ability to manufacture fine features, ability to enhance functionality, reduce lead times, minimize sub-components, minimize weight, and expand supply chains [3].

However, these advantageous are typically overshadowed by the process tendency to generate flaws, such as porosity, distortion, and large part-to-part variation in safety crucial

application [4, 5]. To mitigate these shortcomings, the objective of this work is to detect the onset of flaw formation in LPBF parts using acoustic emission (AE) sensing. These AE sensors are passive sensors attached to the substrate and captures the acoustic waves generated from the laser sintering. The hypothesis of this work is that both flaws and processing parameters will have a fundamental effect on the acoustic waveform traveling through the sample.

As visualized in FIGURE 1(a), the input energy from the laser generates acoustic waveforms that are transmitted to the AE sensors through the solid medium of the deposited material. If the input energy is increased or decreased there should be a corresponding change in the generated acoustic waveform. Likewise, when the generated acoustic waveform interacts with a void in the sample, for instance, either in the form of a crack or pore, the acoustic waveform will have to travel around and through the void which will change the fundamental waveform, visualized in FIGURE 1(b). Additionally, the acoustic waveform does not travel in a linear path to the sensor and can reverberate inside of the sample and through other geometries which will once again changing the acoustic waveform. Therefore, in this work it is imperative to distinguish the different types of acoustic waveforms and correlate them to specific flaws.

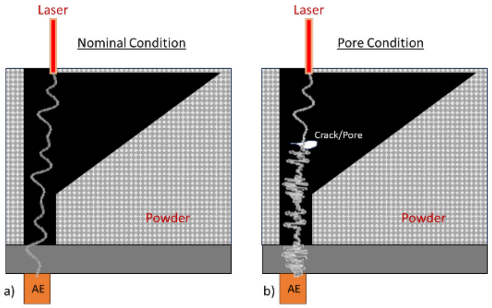

FIGURE 1: A) SHOWCASES THE AE SIGNAL TRANSFERRING THROUGH A NOMINAL PART. B) SHOWCASES THE EFFECTS OF CRACKS AND PORES

2. METHODOLOGY

2.1 Experiments

In this work, 20 simple overhang geometry that are 20 mm tall, 8 mm wide, and has a 45° overhang section, were manufactured using stainless steel 316L (SS-316L). These samples were manufactured at 5 different laser power ranging from -30% laser power (140 W) to +30% laser power (250 W), shown in FIGURE 3. In this work the nominal processing parameters were; laser power 195 W, scan speed 1083 mm·s^{-1}, layer height 20 µm.

To monitor the onset of flaw formation a multi-sensor suite was installed on the EOS M290 LPBF machine at the Commonwealth Center for Advanced Manufacturing (CCAM), Disputanta, VA [6]. The sensors used in this work were a FLIR long wavelength infrared (IR) camera and four AE piezoelectric sensors coupled to the build plate, visualized in FIGURE 2. The FLIR camera operated continuously at a collection rate of 33 Hz to measure top surface temperatures. The four AE sensors were spaced equidistance from each other (125 mm) in a square formation and collected data at 1 MHz. All sensors are controlled via a LabView program and every frame of data is accurately time stamped.

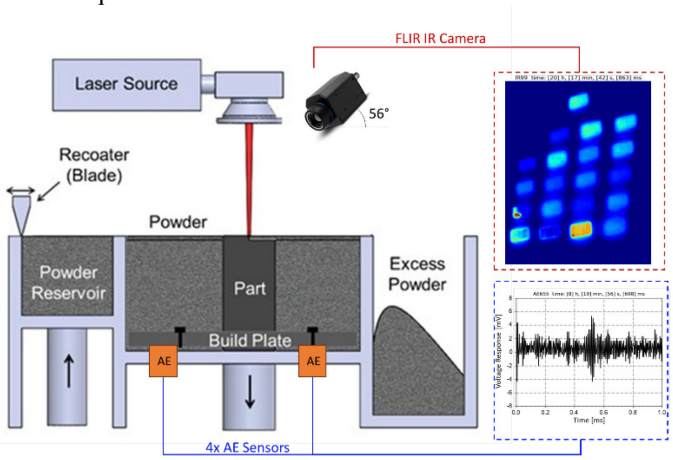

FIGURE 2: VISUALIZATION OF LPBF PROCESS AND THE POSITION OF THE FLIR IR CAMERA AND ACOUSTIC EMISSION SENSORS.

Each power setting had a full support and a reduced support geometry type. As seen in FIGURE 3, most of the full support overhang geometries, power setting 3 through 6, were cancelled early in the printing process. This was done because the support struts were failing and threatened to destroy the entirety of the build. Similarly, the reduced support material had a cancelation at the highest laser power of 250 W. The reason for the high failure rate of the strut material at the high laser powers is because the support struts were printed at the same laser power as the bulk section. Thus, overheating and warpage were prominent in the struts.

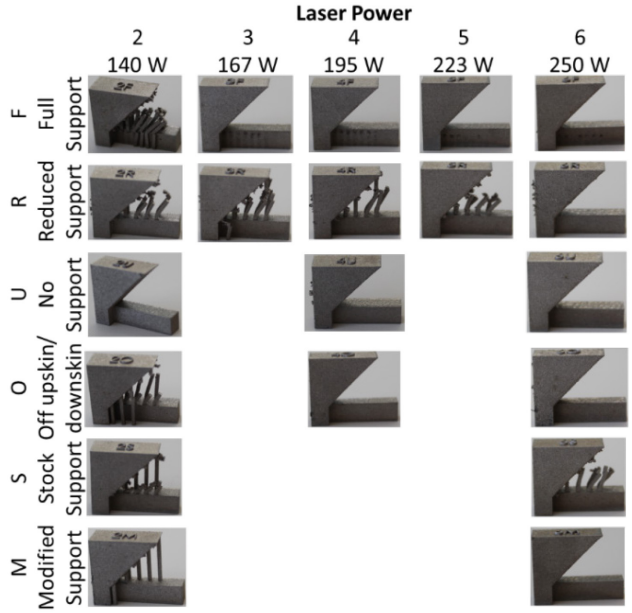

FIGURE 3: 5 LASER POWERS USED IN THIS WORK ALONG WITH THE 6 STUDIES OF GEOMETRY AND CONDITIONS.

Unsupported overhang geometries were only manufactured at 140, 195, and 250 W. This was done due to space restrictions on the build plate that was visible to all the sensors. The three extreme conditions were selected in this study to get a wholistic understanding of heat accumulation and their effects.

All other parameter changes studied in this work were done using the reduced support geometry. Power conditions 2, 4, & 6 were manufactured with the up skin and down skin parameters turned off to study the effects of these parameters, denoted with O in FIGURE 3. Then power conditions 2 and 4 were manufactured with the support struts being printed using stock EOS printing parameters at 195 W, denoted with S in FIGURE 3. Finally, power condition 2 and 4 were manufactured using modified laser power for the strut material based on the percentage change in laser power of the bulk material.

As visualized in FIGURE 3, many of the support structures that were designed were either cancelled by the operator early in the build or had failures. These failures usually came in the form of minor warpage on the support struts, leading to recoater interaction that bent the struts over. These recoater interactions generally occurred at merge points on the overhang when the struts would merge with the under skin of the overhang.

3. PROCESS MONITORING

3.1 Acoustic Emission Feature Extraction

Prior to any data processing, a fundamental understanding of how the AE waveform is affected by the processing conditions of the LPBF process is needed. Depicted in FIGURE 4(a) is the raw acoustic signal for 1 ms when the laser is turned off. It can be observed that during the laser off condition the AE voltage response oscillates between 0-1 mV with a resolution of 1 mV. Found in FIGURE 4(b) is the voltage response for 1 ms when the laser power is set to its lowest input of 140 W. At this processing state, the voltage response increases consistently up to 2 mV and occasionally 3 mV. Finally, at the highest input power of 250 W, the voltage response from the AE sensor increases consistently up to 3 mV and occasionally up to 6 mV, shown in FIGURE 4(c).

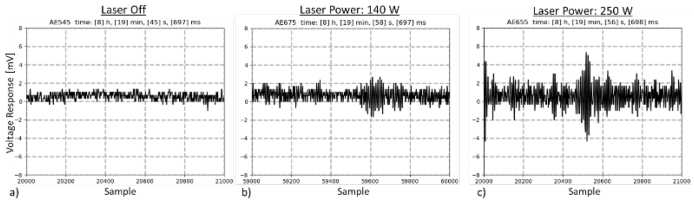

FIGURE 4: EXAMPLE OF THE RAW AE DATA COLLECTED WHEN THE LASER IS OFF, AT A LOW LASER POWER, AND AT A HIGH LASER POWER.

In the most extreme conditions, a simple correlation can be seen in the raw AE data. However, small changes in the processing conditions, and flaw formation are still unobservable simply using the raw AE data. To overcome this limitation, this work will use wavelet multi-resolution decomposition and to analyze the data in the frequency domain. The wavelet decomposition method was chosen because of its ability to accommodate non-stationary and nonlinear data [7].

To perform wavelet analysis, every 33 ms of data from the AE sensors was deconstructed using the biorthogonal 3.3 deconstruction wavelet into its 8 base frequencies (octaves) and the adjusted signal. The biorthogonal 3.3 wavelet was chosen heuristically after evaluation of several other (deconstruction) wavelets and due to its success in our previous works in deconstructing acoustic signature [8]. With each 33 ms of data deconstructed into eight octaves, the relative energy of each octave was calculated using the following equation:

$$E_{o,i} = \sqrt{\frac{\sum D_{o,i,s}^2}{length(D_{o,i})}} \quad (1)$$

Where E is the energy of octave o for every 33 ms window i, and D is each data point in the deconstructed signal. This process of extracting the energy for every octave of 33 ms raw AE data was repeated for the entire duration of a layer being deposited.

After heuristic analysis, the third octave, centered around 333 kHz response, was determined to have the highest correlation with laser interactions. The visualization of this octave's energy response throughout an entire layer is shown in FIGURE 5. First, there is a large frequency response at the start and end of every layer across all the octaves analyzed shown in red. These spikes correlate to when the recoater blade is raking a new layer of powder over the build plate.

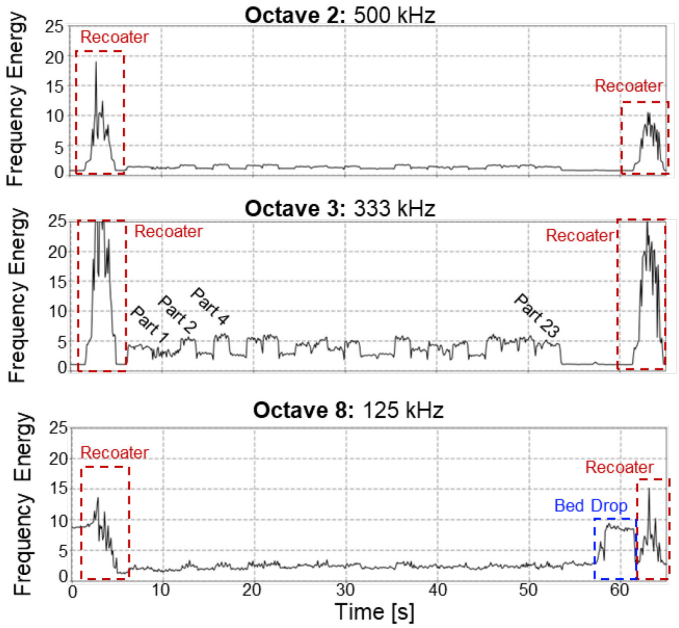

FIGURE 5: RESULTANT WAVELET INTENSITY TIME SERIES FOR AN EXAMPLE LAYER. EACH OF THE FUNDAMENTAL PHENOMENA CAN BE SEEN DURING THIS PROCESS ACROSS THE THREE EXAMPLE OCTAVES BEING DISPLAYED.

In between these spikes exists variation in the energy response which correlates with the sintering of the parts on the build plate. Each part being sintered has its own response and variation which is the most prominent in the third octave centered at 333kHz. In addition, even the bed lowering can be

observed in the signal which is most prominent in the lower frequency response of 125 kHz, demarcated in blue. Due to the third octave's high correlation with the lasing process, compared to the other octaves, this octave's energy response was used for the resultant analysis and flaw correlation.

3.2 Correlating AE Features to Build Plate Position

While the third octave energy response can be used as a monitoring statistic in time, it is not currently possible to correlate the 1D time series to flaw formations on the manufactured sample as it is not spatially localized. To overcome this limitation, a novel form of sensor fusion was implemented. The key idea is to use the time stamped spatial information contained in the IR images, to synchronize the AE data to specific locations on the part.

In this work, the IR camera captured a frame of thermal data every 33 ms, the same temporal resolution as the AE energy extraction discussed in the previous section. Using the IR images, the position of the laser spot can be extracted every 33 ms by tracking the pixel with maximum relative temperature. The corresponding AE response is then mapped to the build plate using the extracted location from the IR image. This process of giving each time step of the AE frequency energy an XY position on the build plate is repeated for the entire layer until a normalized heat map of AE frequency energy data is generated.

These XY heatmaps of AE intensity can then be stacked and a composited XZ view of each sample can be observed in FIGURE 6. Here the effect of build height on the AE frequency energy can be observed for un-supported parts built under low (140 W), nominal (195 W), and high (250 W) laser power samples. As evident from FIGURE 6, as the input energy increases so does the resultant AE signal. A majority of increased AE intensity is concentrated on the overhang section, as shown in FIGURE 6. This is caused by a combination heat accumulation in the overhang region, which in turn causes meltpool instability. These laser-material interactions are detected by the AE sensors [9, 10]. The layers of missing data between layers 640-680 are due to leading to error with the acquisition system.

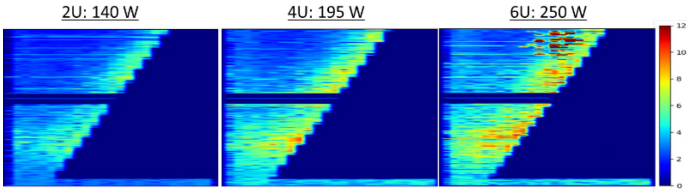

FIGURE 6: THE AE DATA STACKED IN THE XZ DIRECTION AFTER LOCALIZATION. THE EFFECT OF LASER POWER ON THE AE SIGNATURES IS EVIDENT, AS ALSO THE INTENSITY OF THE SIGNATURE IN THE OVERHANG REGION.

4. RESULTS

4.1 Detection of Support Failure

The following demonstrates the ability of the AE signal to detect build failures, such as breaking of supports due to thermal-induced stresses. In FIGURE 7, the compiled AE-derived frequency energy data in XZ direction for sample 2F (fully supported part processed at laser power P=140 W), is plotted and compared to the physical part that was manufactured. In the AE image, clear linear patterns of high intensity are seen. These horizontal lines correlate with the merge points when a row of support struts merges with the overhang section. It is apparent that these merge points generate a high level of AE intensity. These high AE intensities are based on physical phenomena during the manufacturing of the samples. The AE intensity signal detects that there are disturbances prior to the struts being bent to the side. These bent struts are caused by a recoater crash during merge point 4. In addition, there are multiple examples of bent struts and recoater contact events. The recoater contact events occur when the recoater blade interacts with a support strut and displaces it a few hundred micrometers out of place. This minor displacement is not enough to generate a complete failure; however, it is enough to generate a physical error in the sample. The AE signal detects this error before it cascades into a major build failure, such as a recoater crash.

After the catastrophic failure, when the struts were displaced by a recoater crash, there are little to no AE signal in the strut sections due to there being no physical connection between the part and open powder. Then high levels of AE intensity are found in the strut sections when globular material is seen on the manufactured sample. The locational AE frequency energy successfully detects anomalous processing conditions prior to the recoater interference without any complex processing.

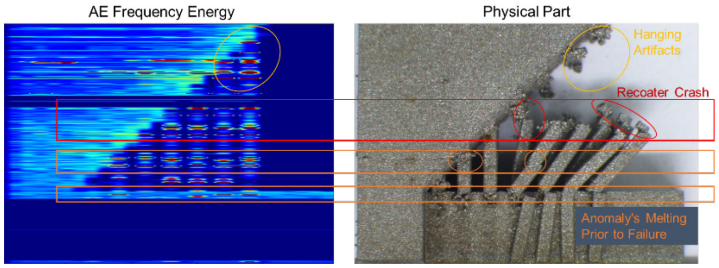

FIGURE 7: SHOWCASING THAT THE AE DATA DETECTED FAILURE IN THE STRUTS PRIOR TO THE RECOATER BLADE BENDING THE SAMPLES.

4.2 Correlation of AE signature with Laser Power and Surface Roughness

In addition to detecting anomalous processing leading to build failures, the average AE frequency energy for each laser power setting was compared and correlated to the surface roughness. First, the average acoustic frequency energy for the first 10 layers to perform this comparison. These first 10 layers were chosen as the baseline as they are the layers closest to the substrate and therefore the layers closest to the AE sensors, ensuring no compounding distance effects. Additionally, these layers occur prior to any flaw formation in the samples, therefore avoiding other compounding effects.

Visualized in FIGURE 8(a), there is a clear linear correlation between the average AE frequency energy and the input laser power, with regression $R^2 \sim 99\%$. This implies that as the input

energy increases, the energy received by the AE sensor also increases.

Continuing with the analysis, the surface under the overhang region with no support material was measured with a confocal microscope. Is was found that the surface finish is correlated to the AE frequency energy feature. To explain further, the average AE intensity within 1 mm of the under skin was calculated and plotted against the average surface roughness, shown in FIGURE 8(b). There is a clear linear correlation between the average surface roughness and the average AE frequency energy feature with a $R^2 \sim 87\%$. This relationship is significant because when the surface roughness of the under skin is compared directly to the laser power, the liner relationship drops to an R^2 of 78% [11]. This implies that the AE signatures detect the stochastic events that occur in the LPBF process and are closely related to flaw formation.

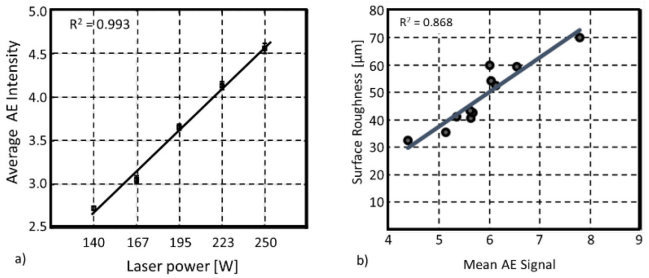

FIGURE 8: THERE IS A LINEAR CORRELATION BETWEEN THE AVERAGE AE INTENSITY AND (A)THE LASER POWER WITH AN R^2 OF 99%, (B) SURFACE ROUGHNESS OF ~87%.

5. CONCLUSION

This work is one of the few in the literature to use AE sensing for process monitoring in LPBF [12]. It demonstrates a fundamental correlation between passive AE sensing and part quality in the LPBF process. By performing computationally tractable wavelet-based decomposition and frequency analysis, correlations to part failure and recoater interactions become apparent. Additionally, clear linear correlations between the acoustic frequency response and both input laser power and surface roughness were made with an $R^2 \sim 99\%$ of 87%, respectively. Pertinently, the proposed methodology in this work is capable of detecting the onset of flaw formation prior to failure and prior to traditional top surface sensors.

In our future works, more complex frequency analysis will be performed to better understand the sub-surface effects in the LPBF process. Additionally, higher fidelity IR cameras at a higher frame rate will be used to achieve a higher spatial resolution of the resultant locational acoustic intensity features. Finally, the developed acoustic monitoring approach will be used to correlate to the evolved microstructure in LPBF parts.

ACKNOWLEDGEMENTS

This work was supported by the National Science Foundation (NSF) for funding his work under awards CMMI-2309483/1752069, OIA-1929172,PFI-TT 2322322/2044710, CMMI-1920245, ECCS-2020246, CMMI-1739696, and CMMI-1719388. Experiments were conducted at the Commonwealth Center for Advanced Manufacturing (CCAM).

REFERENCES

1. Blakey-Milner, B., et al., *Metal additive manufacturing in aerospace: A review.* Materials & Design, 2021. **209**: p. 110008.
2. Chen, H., et al., *Enhanced tensile ductility of an additively manufactured AlSi10Mg alloy by reducing the density of melt pool boundaries.* Scripta Materialia, 2022. **221**: p. 114954.
3. DebRoy, T., et al., *Additive manufacturing of metallic components – Process, structure and properties.* Progress in Materials Science, 2018. **92**: p. 112-224.
4. Diegel, O., A. Nordin, and D. Motte, *Design for Metal AM*, in *A Practical Guide to Design for Additive Manufacturing*. 2019, Springer. p. 121-155.
5. Dreiseitl, S. and L. Ohno-Machado, *Logistic regression and artificial neural network classification models: a methodology review.* Journal of Biomedical Informatics, 2002. **35**(5): p. 352-359.
6. Plotnikov, Y., et al., *Synchronous multi-sensor monitoring for additive manufacturing.* Mater. Eval, 2020. **78**(2): p. 193-202.
7. Shensa, M.J., *The discrete wavelet transform: wedding the a trous and Mallat algorithms.* IEEE Transactions on signal processing, 1992. **40**(10): p. 2464-2482.
8. Bevans, B., et al., *Monitoring and flaw detection during wire-based directed energy deposition using in-situ acoustic sensing and wavelet graph signal analysis.* Materials & Design, 2023. **225**: p. 111480.
9. Montazeri, M. and P. Rao, *Sensor-Based Build Condition Monitoring in Laser Powder Bed Fusion Additive Manufacturing Process Using a Spectral Graph Theoretic Approach.* Journal of Manufacturing Science and Engineering, 2018. **140**(9).
10. Yavari, R., et al., *Part-scale thermal simulation of laser powder bed fusion using graph theory: Effect of thermal history on porosity, microstructure evolution, and recoater crash.* Materials & Design, 2021. **204**: p. 109685.
11. Snyder, J.C. and K.A. Thole, *Understanding Laser Powder Bed Fusion Surface Roughness.* Journal of Manufacturing Science and Engineering, 2020. **142**(7).
12. Prem, P.R., et al., *A Review on Application of Acoustic Emission Testing During Additive Manufacturing.* Journal of Nondestructive Evaluation, 2023. **42**(4): p. 96.